

PROJECTED CHANGES IN CALIFORNIA'S PRECIPITATION INTENSITY-DURATION-FREQUENCY CURVES

A Report for:

California's Fourth Climate Change Assessment

Prepared By:

Amir AghaKouchak¹, Elisa Ragno¹, Charlotte Love¹, Hamed Moftakhari¹

1 University of California, Irvine

DISCLAIMER

This report was prepared as the result of work sponsored by the California Energy Commission. It does not necessarily represent the views of the Energy Commission, its employees or the State of California. The Energy Commission, the State of California, its employees, contractors and subcontractors make no warrant, express or implied, and assume no legal liability for the information in this report; nor does any party represent that the uses of this information will not infringe upon privately owned rights. This report has not been approved or disapproved by the California Energy Commission nor has the California Energy Commission passed upon the accuracy or adequacy of the information in this report.



Edmund G. Brown, Jr., *Governor*

August 2018

CCCA4-CEC-2018-005

ACKNOWLEDGEMENTS

This study was supported by the California Energy Commission Contract No. 500-15-005. We thank Daniel Cayan, David Pierce, and Julie Kalansky from Scripps Institution of Oceanography, University of California, San Diego, for providing downscaled climate model simulations. The authors also appreciate feedback and comments from California's Fourth Climate Change Assessment PIs, Co-PIs, and program managers during the quarterly meetings throughout the project.

PREFACE

California's Climate Change Assessments provide a scientific foundation for understanding climate-related vulnerability at the local scale and informing resilience actions. These assessments contribute to the advancement of science-based policies, plans, and programs to promote effective climate leadership in California. In 2006, California released its First Climate Change Assessment, which shed light on the impacts of climate change on specific sectors in California and was instrumental in supporting the passage of the landmark legislation Assembly Bill 32 (Núñez, Chapter 488, Statutes of 2006), California's Global Warming Solutions Act. The Second Assessment concluded that adaptation is a crucial complement to reducing greenhouse gas emissions (2009), given that some changes to the climate are ongoing and inevitable, motivating and informing California's first Climate Adaptation Strategy released the same year. In 2012, California's Third Climate Change Assessment made substantial progress in projecting local impacts of climate change, investigating consequences to human and natural systems, and exploring barriers to adaptation.

Under the leadership of Governor Edmund G. Brown, Jr., a trio of state agencies jointly managed and supported California's Fourth Climate Change Assessment: California's Natural Resources Agency (CNRA), the Governor's Office of Planning and Research (OPR), and the California Energy Commission (Energy Commission). The Climate Action Team Research Working Group, through which more than 20 state agencies coordinate climate-related research, served as the steering committee, providing input for a multi-sector call for proposals, participating in selection of research teams, and offering technical guidance throughout the process.

California's Fourth Climate Change Assessment (Fourth Assessment) advances actionable science that serves the growing needs of state and local-level decision-makers from a variety of sectors. It includes research to develop rigorous, comprehensive climate change scenarios at a scale suitable for illuminating regional vulnerabilities and localized adaptation strategies in California; datasets and tools that improve integration of observed and projected knowledge about climate change into decision-making; and recommendations and information to directly inform vulnerability assessments and adaptation strategies for California's energy sector, water resources and management, oceans and coasts, forests, wildfires, agriculture, biodiversity and habitat, and public health.

The Fourth Assessment includes 44 technical reports to advance the scientific foundation for understanding climate-related risks and resilience options, nine regional reports plus an oceans and coast report to outline climate risks and adaptation options, reports on tribal and indigenous issues as well as climate justice, and a comprehensive statewide summary report. All research contributing to the Fourth Assessment was peer-reviewed to ensure scientific rigor and relevance to practitioners and stakeholders.

For the full suite of Fourth Assessment research products, please visit www.climateassessment.ca.gov. This report contributes to energy and infrastructure resilience by providing projected changes in extreme precipitation events in California.

ABSTRACT

Traditionally, infrastructure design and rainfall-triggered landslide models rely on the notion of stationarity, which assumes that the statistics of hydroclimatic extremes (e.g., rainfall, streamflow, etc.) do not change significantly over time. However, during the last century, we have observed a warming climate with more intense precipitation extremes in some regions, likely due to increases in the water holding capacity of the atmosphere. Consequently, infrastructure and natural slopes will likely face more severe climatic conditions, with potential human and socioeconomic consequences. Here, we outline a framework for quantifying climate change impacts on natural and man-made infrastructure using bias-corrected multi-model simulations of historical and projected precipitation extremes. The approach evaluates changes in rainfall intensity-duration-frequency (IDF) curves and their uncertainty bounds using a non-stationary model based on Bayesian inference. We show that highly populated areas across California may experience extreme precipitation that is more intense and twice as frequent, relative to historical records, despite the expectation of unchanged annual mean precipitation. Since IDF curves are widely used for infrastructure design and risk assessment, the proposed framework offers an avenue for assessing infrastructure resilience and landslide hazard in a warming climate.

Keywords: Precipitation, Intensity-Duration-Frequency, Extremes, Climatic Change, IDF

Please use the following citation for this paper:

AghaKouchak, Amir, Elisa Ragno, Charlotte Love, and Hamed Moftakhari. (University of California, Irvine). 2018. *Projected changes in California's precipitation intensity-duration-frequency curves*. California's Fourth Climate Change Assessment, California Energy Commission. Publication Number: CCCA4-CEC-2018-005.

HIGHLIGHTS

- The report presents intensity-duration-frequency curves for various locations in California based on multi-model future climate model simulations (2050-2099 relative to 1950-1999). Intensity-Duration-Frequency curves are widely used in infrastructure design and risk assessment, and the curves presented here have potential application in adapting infrastructure design and risk assessment to incorporate projected changes in extreme precipitation.
- Increase in intensity, duration, and frequency of extreme precipitation can adversely impact the integrity of infrastructure, particularly natural and engineered slopes. Indeed, severe rainfall causes flooding, landslides, soil erosion and jeopardizes functionality or integrity of infrastructure systems such as natural gas pipelines.
- The report presents a new way of investigating and communicating the risk of hazardous climatic conditions by calculating the expected future return period of historical events, a useful metric for planning and decision making.
- Extreme precipitation is expected to increase across most cities in California based on the current multi-model climate simulations presented in this report.
- Climate model simulations under the RCP8.5 project that in the future, the frequency of what is currently a 50-year event could double in both Southern California (i.e., San Diego, and Santa Barbara) and Northern California (i.e., San Jose and San Francisco). This means that highly populated areas across California may experience extreme precipitation that is more intense and twice as frequent, relative to historical records, despite the expectation that, on average, annual mean precipitation will not change substantially.

TABLE OF CONTENTS

ACKNOWLEDGEMENTS	i
PREFACE	ii
ABSTRACT	iii
HIGHLIGHTS	iv
TABLE OF CONTENTS.....	v
1: Introduction	1
2: Data	2
3: Method	3
4: Results and Discussion	6
5: Conclusions	15
6: References.....	16
APPENDIX A: Detailed Methodology	A-1
APPENDIX B: Tables of Precipitation Intensity-Duration-Frequency	B-1

1: Introduction

Over the past decades, the observed increase in temperatures (e.g. Barnett et al., 1999; Melillo et al., 2014; Diffenbaugh et al., 2015; Fischer and Knutti, 2015), mainly driven by anthropogenic activities (Melillo et al., 2014), has altered the hydrological cycle leading to more intense rainfall events (Zhang et al., 2007; Min et al., 2011; Marvel and Bonfils, 2013; Westra et al., 2013; Cheng and AghaKouchak, 2014; Fischer and Knutti, 2016). This in turn, can potentially increase the risk of fluvial and pluvial flooding (Melillo et al., 2014; Pachauri et al., 2014; Moftakhari et al., 2017). In addition, recent studies have shown that, given the expected increase in future precipitation, there is a high chance of substantial impact on landslide activity in natural slopes (Robinson et al., 2017) and on the performance of man-made earthen structures (Vahedifard et al., 2017; Jasim et al., 2017), calling into question the current procedure for infrastructure design and risk assessment.

Design and risk assessment procedures for infrastructure (e.g. levees, dams, roads, sewer and storm water drainage systems) often rely on rainfall Intensity-Duration-Frequency (IDF) curves for estimating the design storm intensity and the corresponding flow. Rainfall IDF curves indicate the magnitude of an extreme event with a certain duration and expected recurrence interval based on historical observations.

The process of estimating IDF curves requires fitting a representative distribution function to the observed rainfall data (Bonnin et al., 2006). Traditionally, the parameters of the distribution function are estimated under the so-called stationary assumption (i.e., time invariant parameters), meaning that no significant changes are expected in the characteristics (e.g., magnitude and frequency) of rainfall extremes over time. However, in a warming climate, the assumption of stationarity may not necessarily be sufficient (Milly et al., 2008).

Several studies have proposed models to address non-stationarity in extreme value analysis (e.g. Katz et al., 2002; Sankarasubramanian and Lall, 2003; Mailhot et al., 2007; Cooley et al., 2007; Huard et al., 2009; Villarini et al., 2009, 2010; Vogel et al., 2011; Zhu et al., 2012; Willems et al., 2012; Katz, 2013; Obeysekera and Salas, 2013; Salas and Obeysekera, 2013; Yilmaz and Perera, 2014; Mirhosseini et al., 2014; Rosner et al., 2014; Cheng and AghaKouchak, 2014; Volpi et al., 2015; Read and Vogel, 2015; Sadegh et al., 2015; Krishnaswamy et al., 2015; Mirhosseini et al., 2015; Mondal and Mujumdar, 2015; Lima et al., 2016; Sarhadi and Soulis, 2017). Most methodologies proposed for evaluating non-stationary IDF curves are largely based on observed historical data assuming no change in statistics of future extreme events (e.g., Cheng and AghaKouchak, 2014). To overcome this limitation, we outline a framework for deriving IDF curves using multi-model climate simulations of the future. Here, we have used the downscaled climate model simulations recommended for California's Fourth Climate Change Assessment. Although climate models exhibit high uncertainty, they offer plausible future scenarios that can be used for estimating changes in IDF curves. When a statistically significant trend is observed in the future projections, the framework estimates IDF curves based on a non-stationary statistical model to account for changes in the statistics of extremes. However, in the case where future projections do not exhibit a significant trend, the proposed framework estimates IDF curves based on the commonly used stationary models.

In this report, we have applied the proposed framework to time series of annual maxima precipitation intensity in a number of urban areas across California. We present updated IDF

curves and quantify the expected changes in frequency of future extreme events (e.g. a 50-yr storm) relative to the past (e.g. baseline events).

2: Data

The report focuses on deriving Intensity-Duration-Frequency (IDF) curves in fourteen urban areas in California (Figure 1). Following the Fourth Assessment guidelines, we use downscaled (LOCA) daily precipitation simulations with a 1/16 degree spatial resolution from the following CMIP5 (Coupled Model Intercomparison Project Phase 5) Global Climate Models (GCMs):

- HadGEM2-ES (warm/dry);
- CNRM-CM5 (cool/wet);
- CanESM2 (middle);
- MICROC5 (complement/cover range of outputs)

The simulations include Representative Concentration Pathways (RCP) 4.5 and 8.5. We consider daily precipitation estimates for 1950-1999 and 2050-2099 to be representative of the historical and future climate, respectively. Given that the focus of this report is on frequency analysis, we have chosen a 50-year baseline to be consistent with the typical length of record used in the current historical IDF curves. Also, we have chosen a 50-year projection period to ensure consistency of sample sizes in the baseline and projection periods.

For each location, we independently analyze daily precipitation products of each GCM to retrieve time series of annual maxima intensity in a water year (October through September, as defined by the United States Geological Survey) for events of 1-day to 7-day duration. It is worth noting that any storm duration can be investigated. Here, we focus on daily duration because the downscaled GCM simulations provided for the Fourth Assessment are daily. A time series of annual maxima is obtained as follows. Let's consider the time series of daily precipitation of the j th water year, $P^j = \{p_1^j, \dots, p_{n_j}^j\}$, where n_j is the number of days in the j th water year. The annual precipitation intensity of a d -day event for the j th water year is:

$$P_{d,max}^j = \max \left\{ \frac{\sum_{t=1}^d p_t^j}{d}, \dots, \frac{\sum_{t=i}^{i+d-1} p_t^j}{d}, \dots, \frac{\sum_{t=n_j-d+1}^{n_j} p_t^j}{d} \right\} \quad (1)$$

The time series of annual maxima is then $P_{d,max} = \{P_{d,max}^1, \dots, P_{d,max}^{ny}\}$, where ny is the total number of water years (49 in this study). For each model, we process the historical simulations and the future projections independently.

Location	Lat.	Long.
	N	W
Eureka	40.81	124.17
Redding	40.59	122.39
Sacramento	38.57	121.49
San Francisco	37.78	122.42
San Jose	37.34	121.89
Fresno	36.74	119.78
Monterey	36.59	121.90
Santa Barbara	34.42	119.70
Ventura	34.28	119.22
Los Angeles	34.04	118.22
Riverside	33.95	117.39
Palm Springs	33.84	116.53
Irvine	33.67	117.79
Temecula	33.49	117.15
Escondido	33.12	117.09
San Diego	32.71	117.16



Figure 1: Location of cities in the State of California where changes in precipitation IDF curves are investigated.

3: Method

Precipitation Intensity-Duration-Frequency (IDF) curves available from the National Oceanic and Atmospheric Administration (NOAA) involve fitting a representative distribution function to observed (historical) extreme precipitation. Two main underlying assumptions have been considered: (i) annual precipitation maxima follow a Generalized Extreme Value (GEV) distribution (see Appendix A.); (ii) the statistics of the distribution are time-invariant (stationarity assumption). The assumption (ii) refers to the expectation of a climate in which precipitation characteristics do not change over time. However, for a more realistic representation of the time series behavior (Cheng and AghaKouchak, 2014) we need to account for changes in the statistics of the extremes if they are significant (Katz, 2013).

Based on the above considerations, we employed time series of annual maxima precipitation intensity explained in Section 2 to retrieve historical and projected IDF curves based on Ragno et al. (2018).

We retrieved historical IDF curves using historical simulations and a stationary GEV distribution to reproduce NOAA IDF curves. Additionally, we retrieved future IDF curves using future projections and a GEV distribution with parameters that change over time (hereafter, non-stationary GEV), to incorporate trends in the data when observed. Indeed, the

non-stationary GEV was used when the Mann-Kendall trend test result detected a statistically significant trend in precipitation (i.e. null-hypothesis of no trend is rejected at a 0.05 level of significance).

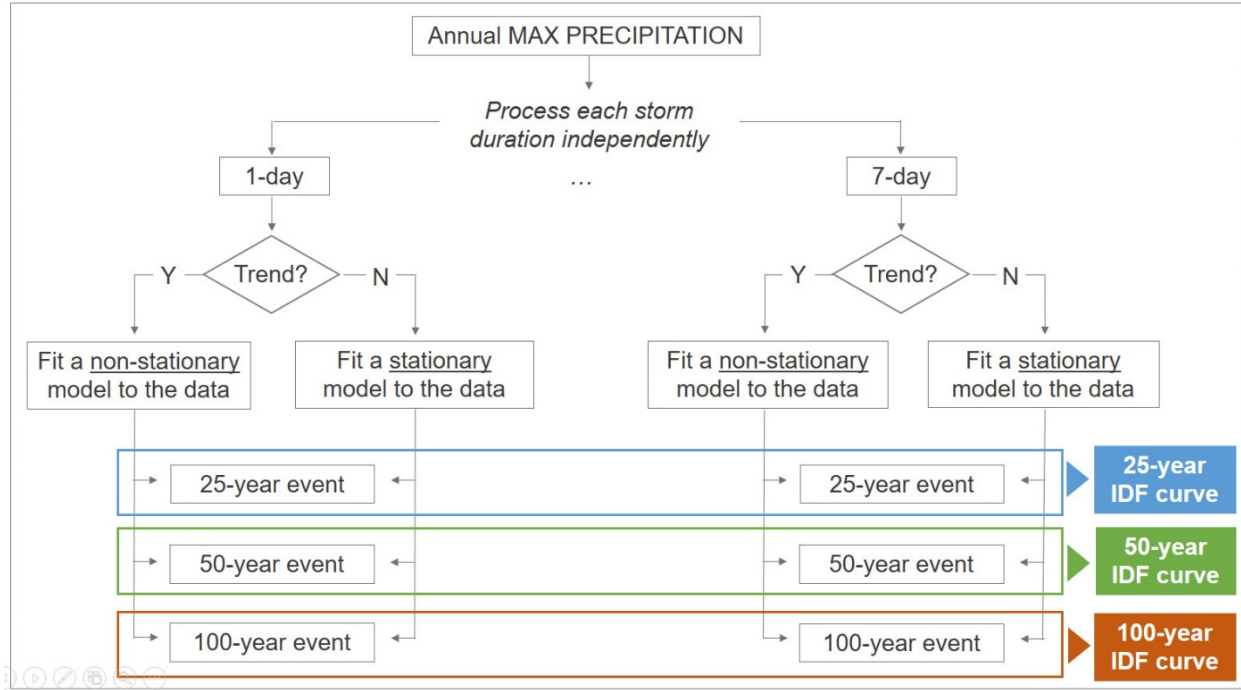


Figure 2. Flow chart indicating the steps for estimating non-stationary Intensity-Duration-Frequency curves.

Figure 2 outlines the procedure for estimating IDF curves. For each duration, a statistical model (stationary/non-stationary) is fitted to the precipitation time series, and the intensities associated with 25-, 50-, 100-yr events are estimated. Afterwards, precipitation intensities are grouped based on their associated return period, and they are plotted as a function of storm duration (1- to 7-day duration) to obtain IDF curves.

We employ the Non-Stationary Extreme Value Analysis (NEVA; Cheng et al., 2014) toolbox to estimate the parameters of the GEV distribution in the case of both stationary and non-stationary analysis (see Appendix A for details). The advantages that NEVA offers include i) flexibility of including the time component to model observed/expected changes, ii) ability of quantifying the uncertainty involved in the estimation procedure using Bayesian inference and the Differential Evolution Markov Chain (DE-MC) approach (see Appendix A for details). The latter becomes even more important in dealing with extreme events, under which it is important to characterize the variability of the estimate through uncertainty analysis.

We first independently calculate the IDF curves for each climate model and then merge them to generate the multi-model ensemble of IDF curves. Finally, for each location and each RCP scenario we obtain the expected IDF curve along with its uncertainty bounds (Figure 3).

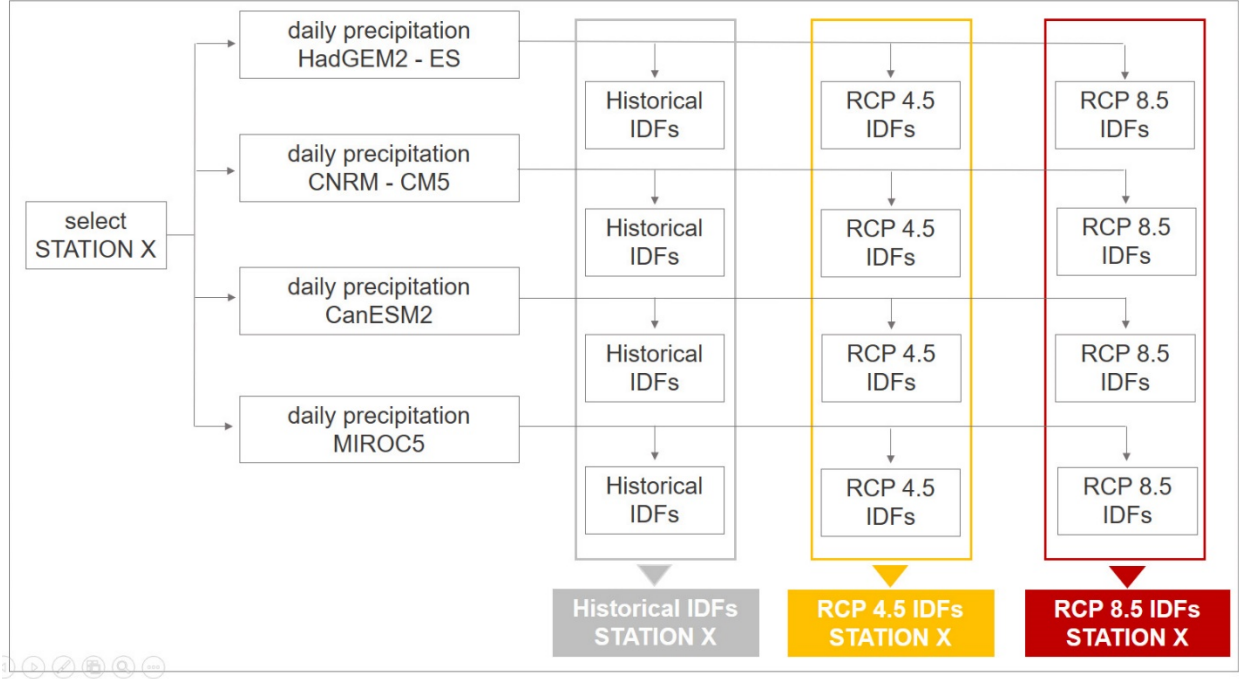


Figure 3. Flow chart indicating the steps to retrieve multi-model ensemble Intensity – Duration – Frequency (IDF) curves for a specific location (i.e. *Station X*). Precipitation from each climatic model is processed independently. The results are then combined to provide a multi-model ensemble of IDF curves. IDF curves are generated following the method explained in Figure 2.

This uncertainty encompasses information about both the inter- (e.g. due to parameter estimation) and intra-model variability (e.g. diversity of GCM simulations). Typically, a bias between the median of historical IDF curves and NOAA IDF curves is expected. This bias stems from the fact that GCMs provide gridded average precipitation, while the current NOAA IDF curves are mainly based on point observations. Gridded area-averaged observations are typically smoother compared to point observations. For this reason, we bias corrected the historical and future IDF curves to make them comparable to the NOAA curves. The bias correction is performed such that the median of the historical IDF curves match the current NOAA IDF curve for a given recurrence interval (Ragno et al., 2018).

Finally, we are interested in quantifying the changes in frequency (i.e., return period) of events in the future relative to the past. From the current NOAA precipitation frequency estimates for a given location, we extract I_T , the intensity of an event with 1-day duration and return period T . I_T is the event that, based on historical data, is considered to occur on average once every T -years. To assess whether the recurrence of an event with intensity equal to I_T is expected to change under future climate scenarios, we extract all return periods with intensity I_T from the ensemble of future return level curves (Figure 4). We then define the expected future return period of the event I_T to be equal to the median of the return periods (T_i) extracted from the IDF curves based on future climate projections. To be conservative, if the expected future return period is higher than the historical one, the latter is taken as the future return period. We evaluate the upper and the lower bounds of the estimated return period to be the 95th and the 5th ensemble quantiles, respectively.

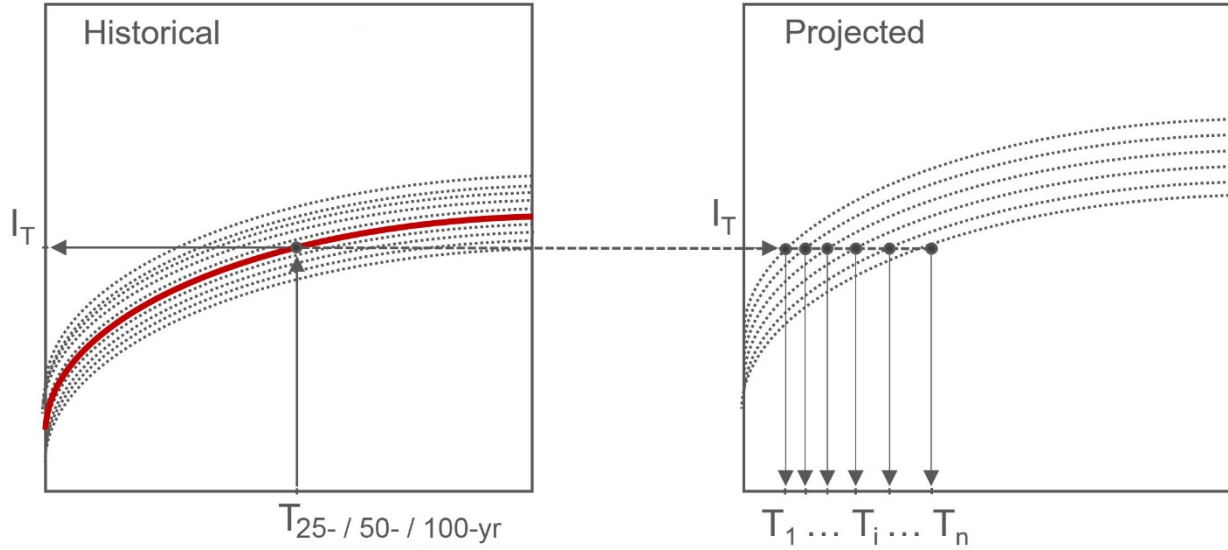


Figure 4: Conceptual explanation of the methodology adopted to quantify changes in the occurrences of historical events under future climate projections (after Ragno et al., 2018). The dotted lines represent the ensemble of solutions from the climate model simulations. The red line represents the ensemble median.

4: Results and Discussion

Under the chosen future scenarios, our results show an overall upward shift of the Intensity-Duration-Frequency (IDF) curves, indicating that more severe events are expected to occur. Figures 5 - 7 and Figures 8 - 10 show IDF curves based on RCP4.5 and RCP8.5 scenarios, respectively. In the presented IDF curves, the proposed non-stationary method is only used when a statistically significant trend is detected in precipitation time series. Interested readers can find the numerical values of the expected IDF curves in Appendix B.

An overall pattern towards more intense precipitation is observable under both RCPs for events with 25-, 50-, and 100-year return periods. In southern California (i.e., Irvine, Riverside, and Escondido) we can observe that, under the RCP4.5, changes in extreme precipitation intensity across different storm durations are smaller in southern California (e.g. Irvine, San Diego) relative to northern California (e.g. Sacramento, San Francisco) – see Figures 5 – 7. The RCP8.5 scenario shows an overall increase in the intensity of extreme events across the state of California. The changes in the intensity of extreme precipitation under the RCP8.5 are more pronounced compared to the RCP4.5.

It is worth noting that precipitation is highly dependent on local climate and so high variability across space is not surprising. Moreover, high uncertainty bounds are mainly associated with the intermodal variability in climate models and the fact that models are subject to biases and uncertainties.

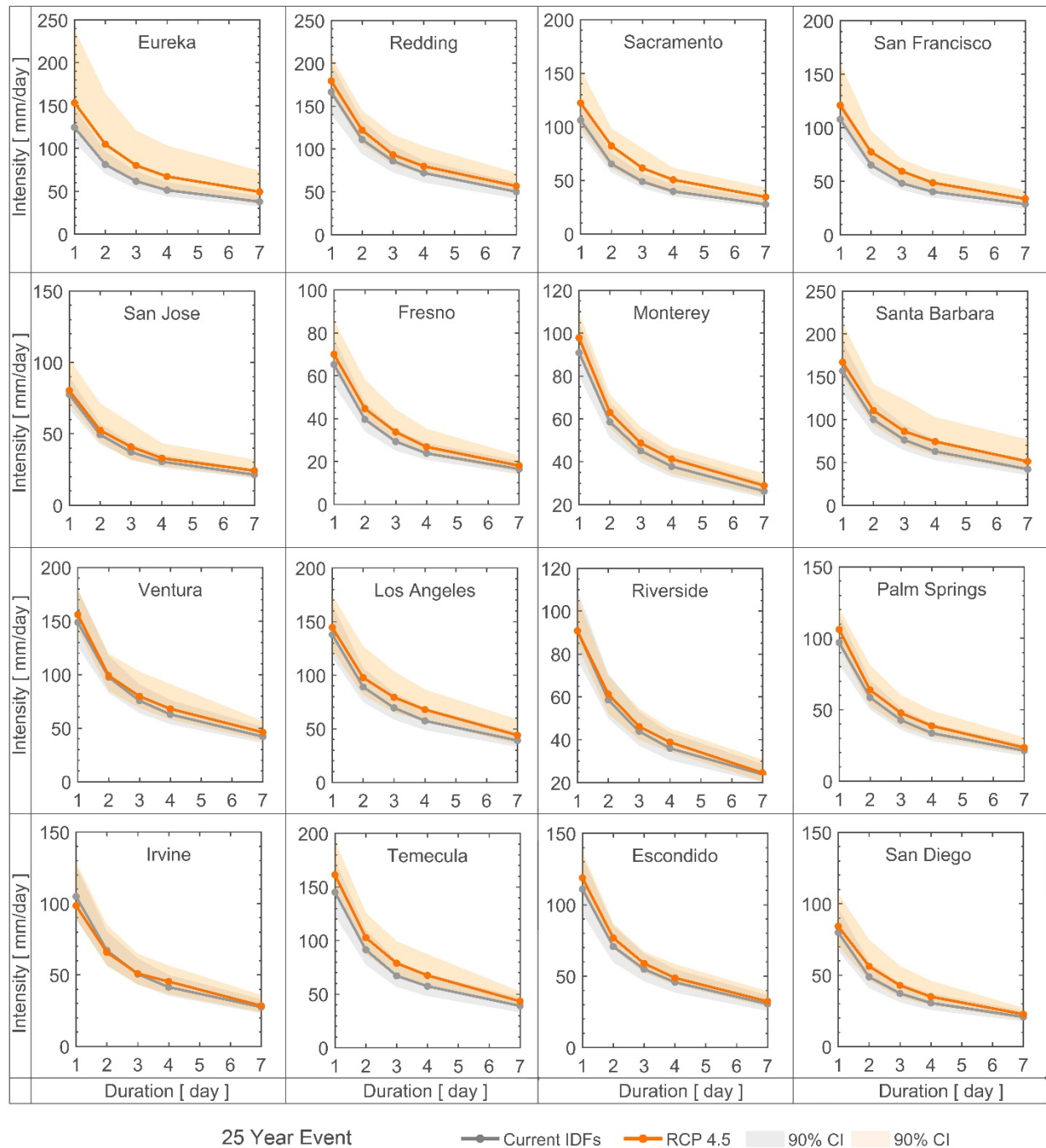


Figure 5: Comparison between the current (grey lines) and future climate (orange lines) 25-yr Intensity-Duration-Frequency (IDF) curves (RCP4.5), along with 90% confidence intervals (after Ragno et al., 2018).

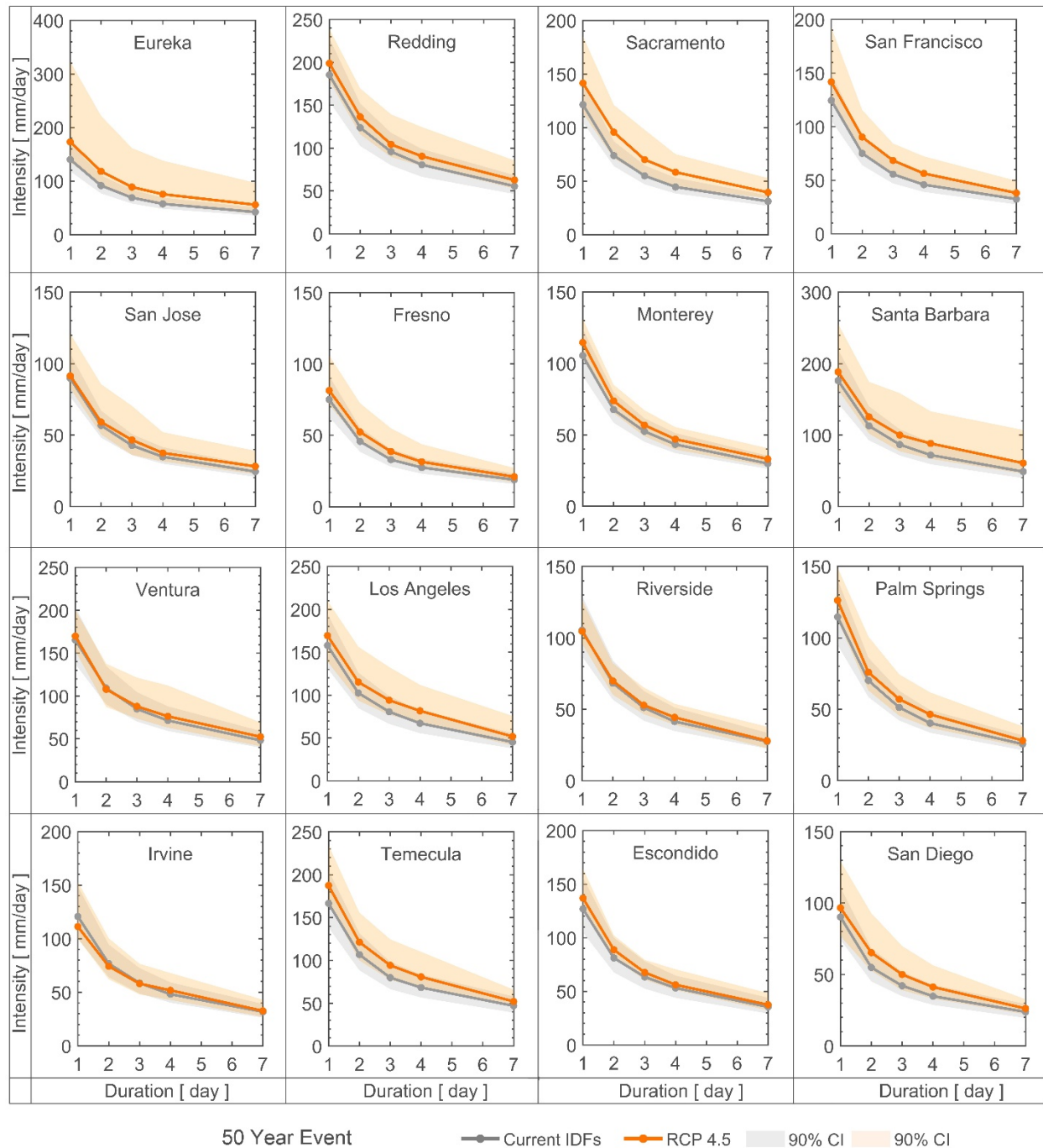


Figure 6: Comparison between the current (grey lines) and future climate (orange lines) 50-yr Intensity-Duration-Frequency (IDF) curves (RCP4.5), along with 90% confidence intervals (after Ragno et al., 2018).

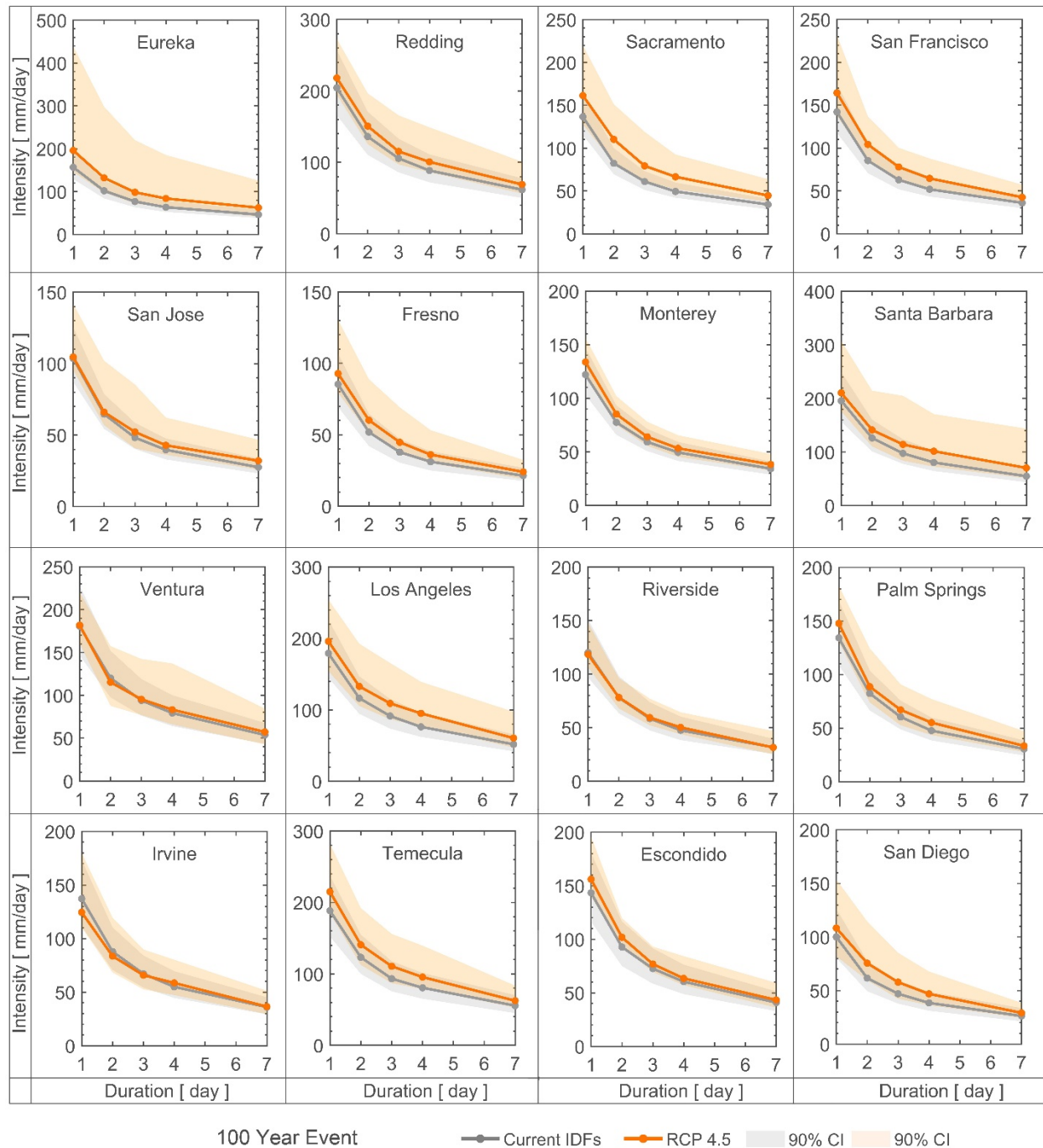


Figure 7: Comparison between the current (grey lines) and future climate (orange lines) 100-yr Intensity-Duration-Frequency (IDF) curves (RCP4.5), along with 90% confidence intervals (after Ragno et al., 2018).

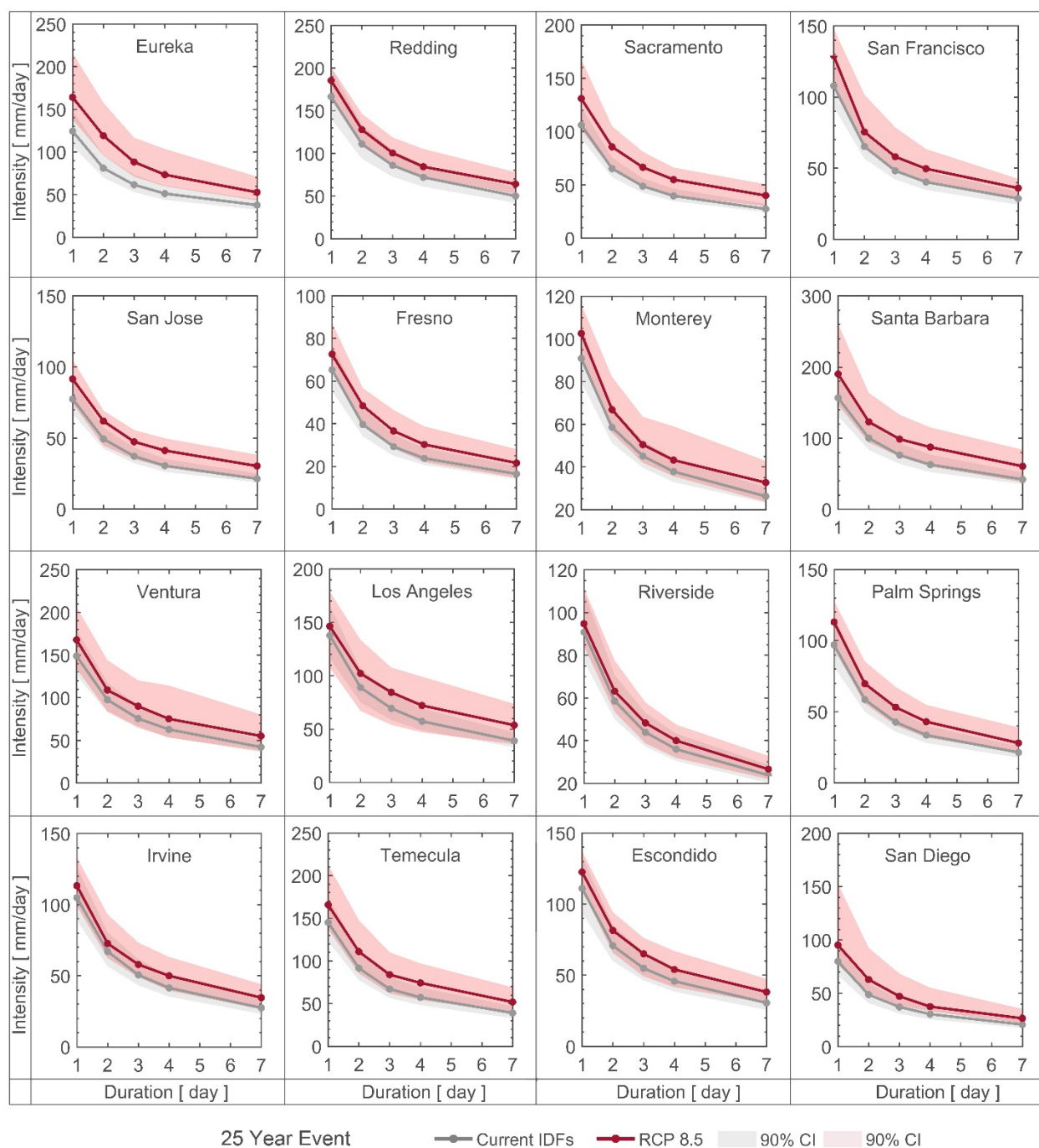


Figure 8: Comparison between the current (grey lines) and future climate (red lines) 25-yr Intensity-Duration-Frequency (IDF) curves (RCP8.5), along with 90% confidence intervals (after Ragno et al., 2018).

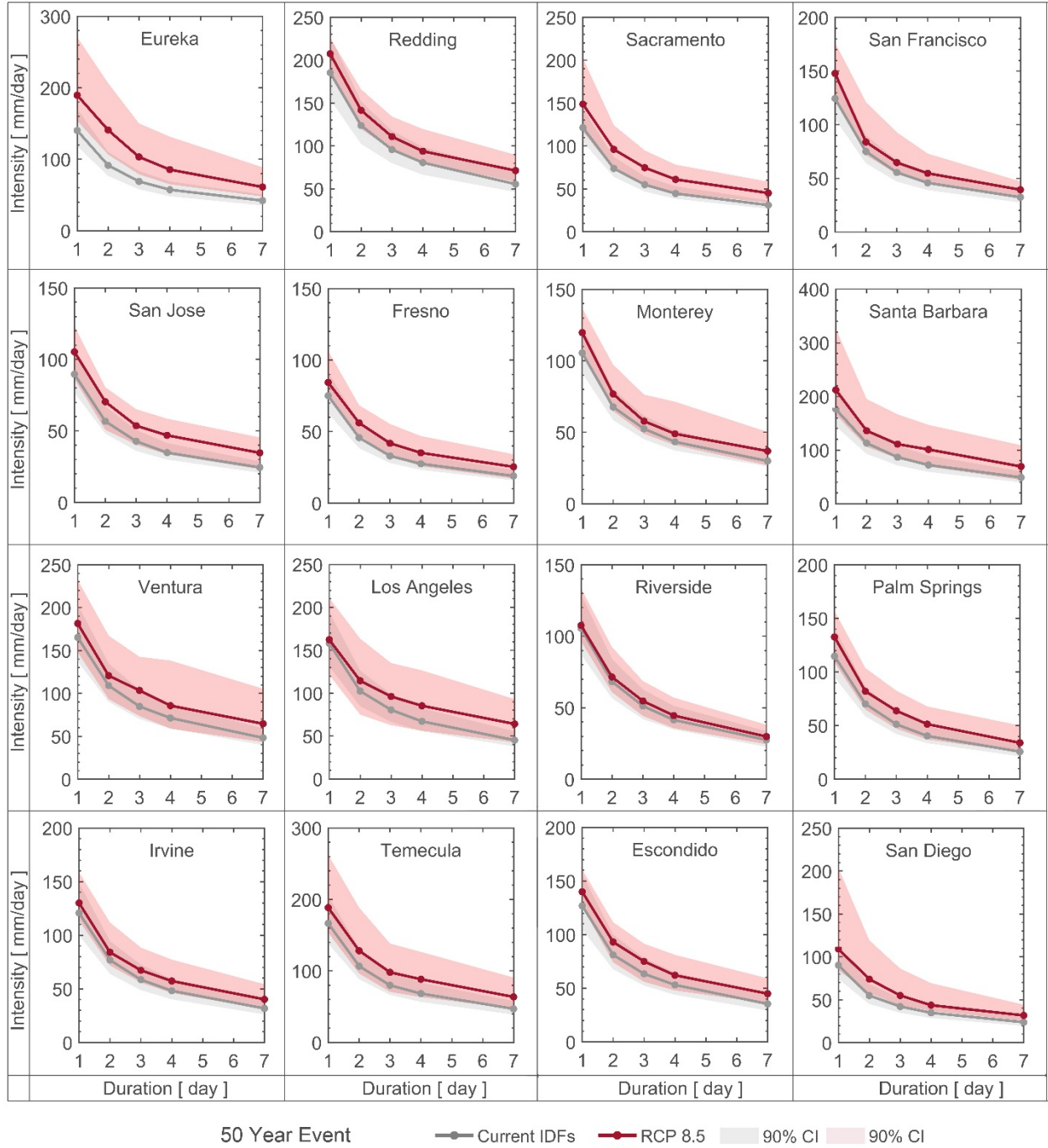


Figure 9: Comparison between the current (grey lines) and future climate (red lines) 50-yr Intensity-Duration-Frequency (IDF) curves (RCP8.5), along with 90% confidence intervals (after Ragno et al., 2018).

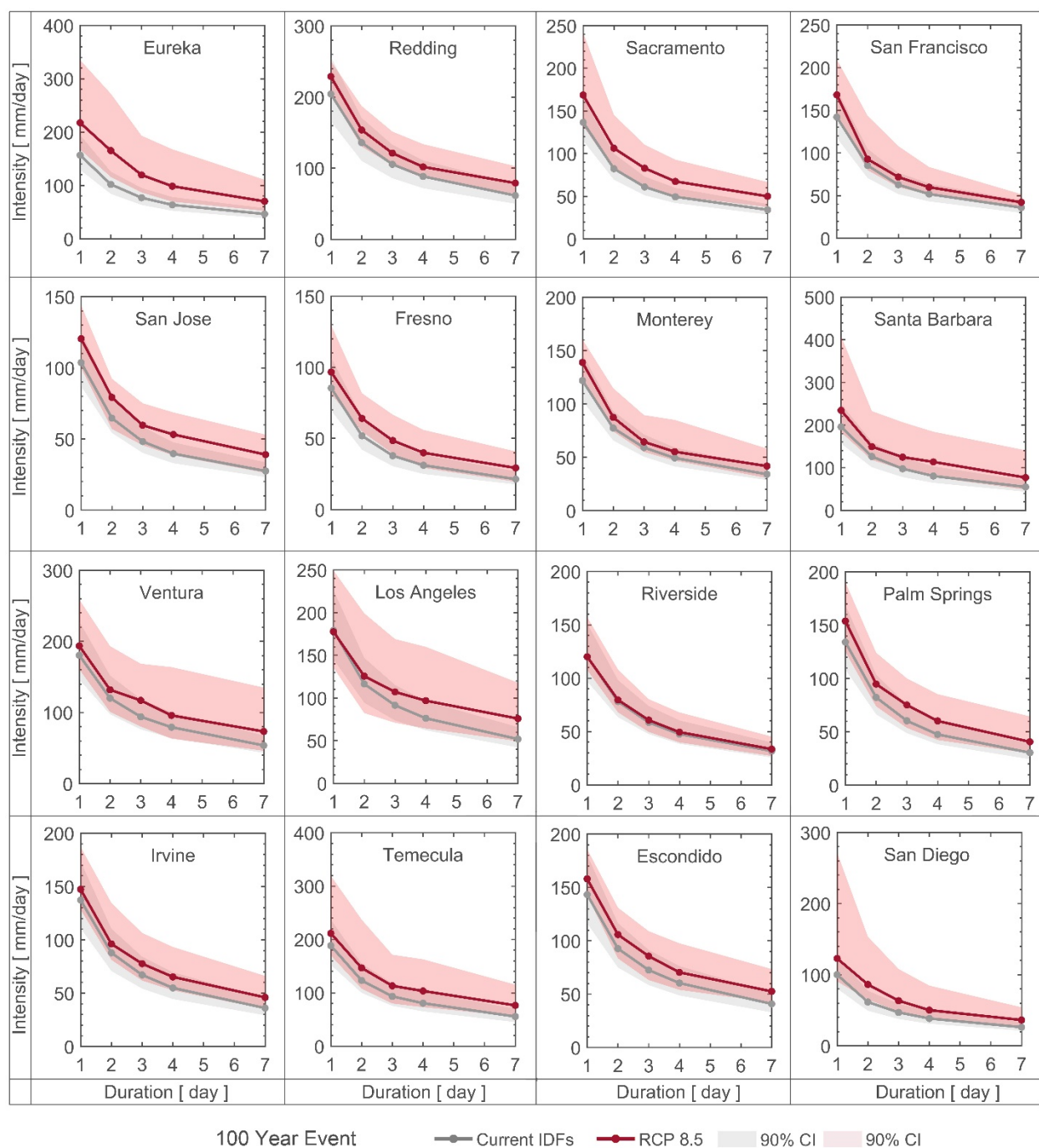


Figure 10: Comparison between the current (grey lines) and future climate (red lines) 100-yr Intensity-Duration-Frequency (IDF) curves (RCP8.5), along with 90% confidence intervals (after Ragno et al., 2018).

After investigating the change in extreme event intensity for a fixed return period, we now explore the changes in frequency of extreme events with 1-day duration for a given event magnitude. Specifically, we choose the intensity of three baseline events corresponding to 25-, 50- and 100-year events (retrieved from current NOAA IDF curves) to estimate their expected recurrence intervals in the future, along with their confidence intervals. Figure 8 illustrates the return periods expected in the future of the baseline events (dots), along with their 90% confidence intervals (gray lines). The results show that extreme events that are expected to occur every 50 or 100 years will likely become more frequent. For example, climate model simulations project that the frequency of a 50-year event in the future will double in San Diego, and Santa Barbara under RCP8.5. The same behavior can be observed in northern California, in San Jose and San Francisco (Figure 11). The high uncertainties in the estimated values reflect the intermodal variability in climate model projections (here, four different climate models) and parameter fitting uncertainties.

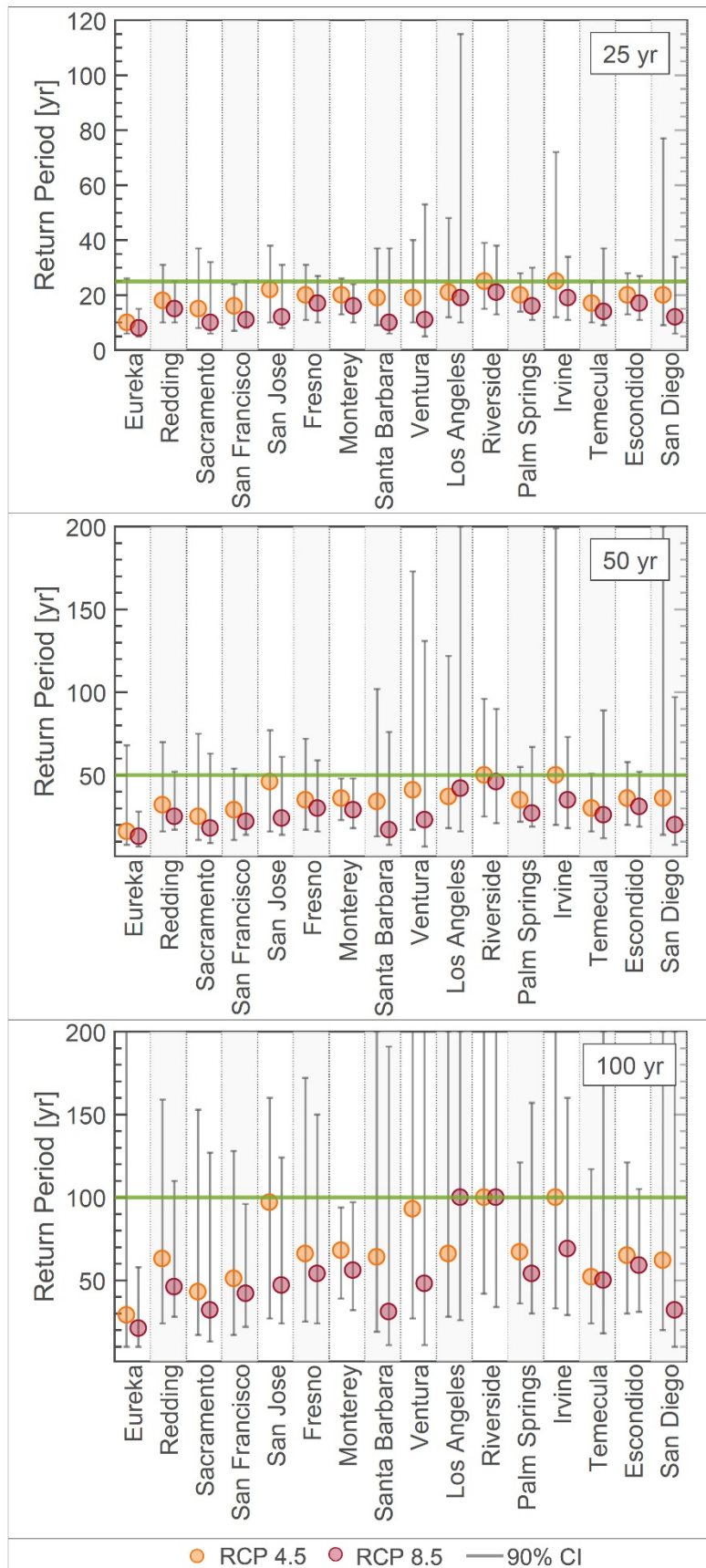


Figure 11: The procedure to obtain expected future return period is explained in Figure 1 (after Ragno et al., 2018). Return periods of future events (orange and red dots), historically associated with return periods of 25-, 50-, and 100-years in California (green lines). Panels a, b, and c show the projected return periods considering two future scenarios: RCP4.5 (orange dots) and RCP8.5 (red dots) along with their 90% confidence interval (gray lines).

5: Conclusions

In this report, we have shown the potential impacts of a warming climate on extreme precipitation intensity and recurrence intervals in California (2050-2099 relative to 1950-1999). The results show that in most cities, extreme precipitation events are projected to intensify. Urban areas in California may struggle against increases in severity and frequency of historically rare events. Increase in intensity, duration, and frequency of extreme precipitation can adversely impact the integrity of infrastructure and natural and engineered slopes. Severe rainfall causes flooding, landslides, and soil erosion and jeopardizes functionality or integrity of infrastructure systems. Infrastructure built with soil (such as earthen dams, levees, or embankments), or the ones that interface with soil (for example roads, bridge, pipelines, and foundations) are often more vulnerable. Recent studies have shown the applicability of the methodology proposed here for assessing the resilience of levees (Jasim et al., 2017) and mechanically stabilized earth (MSE) walls with marginal backfill (Vahedifard et al., 2017) under a changing climate. The IDF curves presented in this report can be used to evaluate the risk of existing infrastructure systems in a changing climate.

6: References

- Barnett, T. P., Hasselmann, K., Chelliah, M., Delworth, T., Hegerl, G., Jones, P., Rasmusson, E., Roeckner, E., Ropelewski, C., Santer, B., and Tett, S. (1999). Detection and attribution of recent climate change: A status report. *Bull. Amer. Meteor. Soc.*, 80(12):2631–2659. 1
- Bonnin, G., Perica, S., Dietz, S., Heim, S., Hiner, L., Maitaria, K., Martin, Deborah Pavlovic, S., Roy, I., Trypaluk, C., Unruh, D., Yan, F., Yekta, M., Zhao, T., Brewer, D., Chen, L.-C., Parzybok, T., and Yarchoan, J. (2006). Precipitation - frequency atlas of the United States. NOAA Atlas 14, 1-10.
- Cheng, L. and AghaKouchak, A. (2014). Nonstationary Precipitation Intensity-Duration-Frequency Curves for Infrastructure Design in a Changing Climate. *Scientific Reports*, 4:7093–. 1,
- Cheng, L., AghaKouchak, A., Gilleland, E., and Katz, R. W. (2014). Non-stationary extreme value analysis in a changing climate. *Climatic Change*, 127(2):353 – 369. 2, 3
- Coles, S. (2001). An introduction to statistical modeling of extreme values. Springer-Verlag, London.
- Cooley, D., Nychka, D., and Naveau, P. (2007). Bayesian Spatial Modeling of Extreme Precipitation Return Levels. *Journal of the American Statistical Association*, 102(479):824–840.
- Diffenbaugh, N. S., Swain, D. L., and Touma, D. (2015). Anthropogenic warming has increased drought risk in California. *Proceedings of the National Academy of Sciences*, 112(13):3931–3936.
- Fischer, E. M. and Knutti, R. (2015). Anthropogenic contribution to global occurrence of heavy-precipitation and high-temperature extremes. *Nature Clim. Change*, 5(6):560–564.
- Fischer, E. M. and Knutti, R. (2016). Observed heavy precipitation increase confirms theory and early models. *Nature Climate Change*, 6:986 – 991.
- Huard, D., Mailhot, A., and Duchesne, S. (2009). Bayesian estimation of Intensity - Duration - Frequency curves and of the return period associated to a given rainfall event. *Stochastic Environmental Research and Risk Assessment*, 24(3):337 – 347.
- Jasim, F. H., Vahedifard, F., Ragno, E., AghaKouchak, A., and Ellithy, G. (2017). Effects of climate change on fragility curves of earthen levees subjected to extreme precipitations. In *Geo-Risk 2017: Geotechnical Risk from Theory to Practice*, Denver, CO.
- Katz, R. W. (2013). Statistical Methods for Nonstationary Extremes. In AghaKouchak, A., Easterling, D., Hsu, K., Schubert, S., and Sorooshian, S., editors, *Extremes in a Changing Climate: Detection, Analysis and Uncertainty*, pages 15 – 37. Springer Netherlands, Dordrecht. 1,
- Katz, R. W., Parlange, M. B., and Naveau, P. (2002). Statistics of extremes in hydrology. *Advances in Water Resources*, 25(8-12):1287–1304.

- Krishnaswamy, J., Vaidyanathan, S., Rajagopalan, B., Bonell, M., Sankaran, M., Bhalla, R. S., and Badiger, S. (2015). Non-stationary and non-linear influence of enso and indian ocean dipole on the variability of indian monsoon rainfall and extreme rain events. *Climate Dynamics*, 45(1):175 – 184.
- Lima, C. H., Kwon, H.-H., and Kim, J.-Y. (2016). A Bayesian beta distribution model for estimating rainfall IDF curves in a changing climate. *Journal of Hydrology*, 540:744 – 756.
- Mailhot, A., Duchesne, S., Caya, D., and Talbot, G. (2007). Assessment of future change in intensity duration frequency (IDF) curves for southern quebec using the Canadian Regional Climate Model (CRCM). *Journal of Hydrology*, 347(12):197 – 210.
- Marvel, K., & Bonfils, C. (2013). Identifying external influences on global precipitation. *Proceedings of the National Academy of Sciences*, 110(48), 19301-19306.
- Melillo, J. M., Richmond, T. T., and Yohe, G. W. (2014). *Climate Change Impacts in the United States: The Third National Climate Assessment*. Technical report, U.S. Global Change Research Program.
- Milly, P. C. D., Betancourt, J., Falkenmark, M., Hirsch, R. M., Kundzewicz, Z. W., Lettenmaier, D. P., and Stouffer, R. J. (2008). Stationarity Is Dead: Whither Water Management? *Science*, 319(5863):573–574.
- Min, S.-K., Zhang, X., Zwiers, F. W., and Hegerl, G. C. (2011). Human contribution to more-intense precipitation extremes. *Nature*, 420:378–381.
- Mirhosseini, G., Srivastava, P., and Fang, X. (2014). Developing Rainfall Intensity-Duration-Frequency Curves for Alabama under Future Climate Scenarios Using Artificial Neural Networks. *Journal of Hydrologic Engineering*, 19(11):04014022.
- Mirhosseini, G., Srivastava, P., and Sharifi, A. (2015). Developing Probability-Based IDF Curves Using Kernel Density Estimator. *Journal of Hydrologic Engineering*.
- Moftakhari, H. R., Salvadori, G., AghaKouchak, A., Sanders, B. F., & Matthew, R. A. (2017). Compounding effects of sea level rise and fluvial flooding. *Proceedings of the National Academy of Sciences*, 114(37), 9785-9790.
- Mondal, A. and Mujumdar, P. (2015). Modeling non-stationarity in intensity, duration and frequency of extreme rainfall over india. *Journal of Hydrology*, 521:217–231.
- Obeysekera, J. and Salas, J. D. (2013). Quantifying the uncertainty of design floods under nonstationary conditions. *Journal of Hydrologic Engineering*, 19(7):1438–1446.
- Pachauri, R. K., Allen, M. R., Barros, V. R., Broome, J., Cramer, W., Christ, R., Church, J. A., Clarke, L., Dahe, Q., Dasgupta, P., et al. (2014). *Climate change 2014: synthesis report*. Contribution of Working Groups I, II and III to the fifth assessment report of the Intergovernmental Panel on Climate Change. IPCC.
- Papalexiou, S. M. and Koutsoyiannis, D. (2013). Battle of extreme value distributions: A global survey on extreme daily rainfall. *Water Resources Research*, 49(1):187–201.

- Ragno E., AghaKouchak A., Love C.A., Cheng L., Vahedifard F., Lima C.H.R., 2018, Quantifying Changes in Future Intensity-Duration-Frequency Curves Using Multi-Model Ensemble Simulations, *Water Resources Research*, in press.
- Read, L. K. and Vogel, R. M. (2015). Reliability, return periods, and risk under nonstationarity. *WaterResources Research*, 51(8):6381–6398.
- Robinson, J. D., Vahedifard, F., and AghaKouchak, A. (2017). Rainfall-triggered slope instabilities under a changing climate: comparative study using historical and projected precipitation extremes. *Canadian Geotechnical Journal*, 54(1):117–127.
- Rosner, A., Vogel, R. M., and Kirshen, P. H. (2014). A risk-based approach to flood management decisions in a nonstationary world. *Water Resources Research*, 50(3):1928 – 1942.
- Sadegh, M., Vrugt, J. A., Xu, C., and Volpi, E. (2015). The stationarity paradigm revisited: Hypothesis testing using diagnostics, summary metrics, and dream(abc). *Water Resources Research*, 51(11):9207–9231.
- Salas, J. D. and Obeysekera, J. (2013). Revisiting the concepts of return period and risk for nonstationary hydrologic extreme events. *Journal of Hydrologic Engineering*, 19(3):554–568.
- Sankarasubramanian, A. and Lall, U. (2003). Flood quantiles in a changing climate: Seasonal forecasts and causal relations. *Water Resources Research*, 39(5):n/a–n/a. 1134.
- Sarhadi, A. and Soulis, E. D. (2017). Time-varying extreme rainfall intensity-duration-frequency curves in a changing climate. *Geophysical Research Letters*, pages 1–10.
- Vahedifard, F., Tehrani, F. S., Galavi, V., Ragno, E., and AghaKouchak, A. (2017). Resilience of mse walls with marginal backfill under a changing climate: Quantitative assessment for extreme precipitation events. *Journal of Geotechnical and Geoenvironmental Engineering*, ASCE.
- Villarini, G., Smith, J. A., and Napolitano, F. (2010). Nonstationary modeling of a long record of rainfall and temperature over rome. *Advances in Water Resources*, 33(10):1256 – 1267.
- Villarini, G., Smith, J. A., Serinaldi, F., Bales, J., Bates, P. D., and Krajewski, W. F. (2009). Flood frequency analysis for nonstationary annual peak records in an urban drainage basin. *Advances in Water Resources*, 32(8):1255 – 1266. 1
- Vogel, R. M., Yaindl, C., and Walter, M. (2011). Nonstationarity: Flood magnification and recurrence reduction factors in the united states1. *JAWRA Journal of the American Water Resources Association*, 47(3):464–474.
- Volpi, E., Fiori, A., Grimaldi, S., Lombardo, F., and Koutsoyiannis, D. (2015). One hundred years of return period: Strengths and limitations. *Water Resources Research*, 51(10):8570–8585.
- Westra, S., Alexander, L. V., and Zwiers, F. W. (2013). Global increasing trends in annual maximum daily precipitation. *Journal of Climate*, 26(11):3904–3918.
- Willems, P., Arnbjerg-Nielsen, K., Olsson, J., and Nguyen, V. (2012). Climate change impact assessment on urban rainfall extremes and urban drainage: Methods and shortcomings. *Atmospheric Research*, 103:106 –118.

- Yilmaz, A. G. and Perera, B. J. C. (2014). Extreme Rainfall Nonstationarity Investigation and Intensity-Frequency-Duration Relationship. *Journal of Hydrologic Engineering*, 19(6):1160–1172.
- Zhang, X., Zwiers, F. W., Hegerl, G. C., Lambert, F. H., Gillett, N. P., Solomon, S., Stott, P. A., and Nozawa, T. (2007). Detection of human influence on twentieth-century precipitation trends. *Nature*, 448(7152):461–465.
- Zhu, J., Stone, M. C., and Forsee, W. (2012). Analysis of potential impacts of climate change on Intensity - Duration - Frequency (IDF) relationships for six regions in the United States. *Journal of Water and Climate Change*, 3:185–196.

APPENDIX A: Detailed Methodology

The cumulative distribution function of the GEV distribution is (Cheng et al., 2014):

$$\Psi(x) = \exp \left\{ - \left(1 + \xi \left(\frac{x - \mu}{\sigma} \right) \right)^{-\frac{1}{\xi}} \right\}$$

where, μ , σ , and ξ are the location parameter representing the center of the distribution, the scale parameter describing the distribution of the data around the center, and the shape parameter that defines the tail behavior of the distribution, respectively.

We employ the Non-Stationary Extreme Value Analysis (NEVA; Cheng et al., 2014) toolbox to estimate the parameters of the GEV distribution in the case of both stationary and non-stationary analysis. The NEVA framework has two main advantages: (i) it is versatile enough to deal with temporal stationary and non-stationary extremes (including annual maxima and extremes over a particular threshold); (ii) it estimates Return Level curves along with their uncertainty bounds through Bayesian inference and the Differential Evolution Markov Chain (DE-MC) approach (Cheng et al., 2014). Indeed, a Bayesian approach allows for uncertainty quantification, which is crucial especially when dealing with small sample size and rare events.

In this study, non-stationarity is characterized by a time-dependent location parameter $\mu(t)$, $\mu(t) = \mu_1 \cdot t + \mu_0$, where the regression parameters μ_1 and μ_0 are calibrated. A longer data set is required to reliably model the σ and ξ variability over time (Coles, 2001; Papalexiou and Koutsoyiannis, 2013), so we assume the scale and shape parameters to be time-invariant, as suggested by Cheng et al., 2014.

We use NEVA to process the historical and future time series of annual maxima and obtain IDF curves of 25-, 50-, and 100-year return periods along with their associated uncertainties. The return period is defined as $1/(1-p)$ where p is the non-exceedance probability of a given event. The intensity of the p -year event is given by:

$$q_p = \left(\left(-\frac{1}{\ln(p)} \right)^\xi - 1 \right) \cdot \frac{\sigma}{\xi} + \hat{\mu}$$

where the location parameter $\hat{\mu} = \text{median}(\mu(t))$ if the null-hypothesis of no monotonic trend is rejected, and $\hat{\mu} = \mu$ elsewhere.

Generally, for the i th-set of GEV parameters, the expected return period T_i is given by $\frac{1}{1-\psi(I_T)}$ where $\psi(I_T)$ is estimated as:

$$\Psi(I_T) = \exp \left\{ - \left(1 + \xi_i \left(\frac{I_T - \mu_i}{\sigma_i} \right) \right)^{-\frac{1}{\xi_i}} \right\}$$

APPENDIX B: Tables of Precipitation Intensity-Duration-Frequency

Table B-1. 25-yr Return Period Intensity-Duration-Frequency curves based on historical records (NOAA) and future climate (RCP4.5 and RCP8.5). The values in the table correspond to the solid lines in Figures 5 and 8. The storm durations indicated are the ones for which NOAA provide the estimates.

<i>25-year Return Period</i>						
<i>LOCATION</i>		<i>1-day mm/day</i>	<i>2-day mm/day</i>	<i>3-day mm/day</i>	<i>4-day mm/day</i>	<i>7-day mm/day</i>
Eureka	NOAA	124.36	81.08	61.57	51.21	37.80
	RCP 4.5	153.14	104.77	80.04	67.14	49.31
	RCP 8.5	164.06	119.08	88.22	73.33	52.70
Redding	NOAA	166.42	110.95	85.95	71.93	49.99
	RCP 4.5	179.33	121.94	93.28	79.84	56.63
	RCP 8.5	185.35	127.83	100.41	84.32	64.01
Sacramento	NOAA	106.07	65.23	48.77	39.62	27.43
	RCP 4.5	122.13	82.08	61.39	50.45	34.31
	RCP 8.5	130.90	85.62	66.48	54.92	39.98
San Francisco	NOAA	107.90	65.23	48.16	40.23	28.65
	RCP 4.5	120.97	77.45	59.38	48.69	33.71
	RCP 8.5	129.05	75.45	58.05	49.61	35.99
San Jose	NOAA	77.42	49.38	37.19	30.48	21.34
	RCP 4.5	80.33	52.45	40.84	32.91	24.18
	RCP 8.5	91.47	61.91	47.35	41.19	30.30
Fresno	NOAA	65.23	39.62	29.26	23.77	16.46
	RCP 4.5	69.97	44.66	33.75	26.78	18.02
	RCP 8.5	72.60	48.42	36.58	30.24	21.59
Monterey	NOAA	90.83	58.52	45.11	37.80	26.21
	RCP 4.5	97.80	63.01	48.69	41.27	28.83
	RCP 8.5	102.52	66.83	50.44	43.19	32.65
Santa Barbara	NOAA	156.67	99.97	76.20	62.79	42.06
	RCP 4.5	166.95	110.57	86.21	74.32	51.17
	RCP 8.5	190.19	122.94	98.64	87.44	60.51
Ventura	NOAA	148.74	97.54	75.59	62.79	42.06
	RCP 4.5	155.93	99.02	79.64	67.98	46.02
	RCP 8.5	167.73	108.96	89.99	75.19	55.06
Los Angeles	NOAA	137.77	89.00	69.49	57.30	39.01
	RCP 4.5	144.52	97.65	79.31	67.84	43.93
	RCP 8.5	146.43	102.12	84.48	72.10	53.67
Riverside	NOAA	90.83	58.52	43.89	35.97	23.77
	RCP 4.5	90.78	61.28	46.13	38.82	24.49

	<i>RCP 8.5</i>	94.75	63.12	48.28	39.97	26.57
Palm Springs	<i>NOAA</i>	96.93	58.52	42.67	33.53	21.34
	<i>RCP 4.5</i>	106.08	63.82	47.65	38.67	23.43
	<i>RCP 8.5</i>	113.01	69.70	53.12	42.93	27.96
Irvine	<i>NOAA</i>	104.85	67.06	50.60	41.45	27.43
	<i>RCP 4.5</i>	98.43	65.77	50.91	45.33	28.40
	<i>RCP 8.5</i>	113.29	72.69	57.90	49.96	34.58
Temecula	<i>NOAA</i>	145.08	91.44	67.06	57.30	39.01
	<i>RCP 4.5</i>	161.32	102.76	78.84	67.44	43.31
	<i>RCP 8.5</i>	165.76	110.86	83.87	74.25	51.82
Escondido	<i>NOAA</i>	110.95	70.71	54.86	45.72	30.48
	<i>RCP 4.5</i>	118.78	76.77	58.87	48.72	32.33
	<i>RCP 8.5</i>	122.49	81.44	65.01	53.99	38.13
San Diego	<i>NOAA</i>	79.86	48.77	37.19	30.48	20.73
	<i>RCP 4.5</i>	84.20	56.16	42.81	34.88	22.61
	<i>RCP 8.5</i>	95.25	62.92	47.19	37.55	26.53

Table B-2. 50-yr Return Period Intensity-Duration-Frequency curves based on historical records (NOAA) and future climate (RCP 4.5 and RCP 8.5). The values in the table correspond to the solid lines in Figures 6 and 9. The storm durations indicated are the ones for which NOAA provide the estimates.

<i>50-year Return Period</i>						
<i>LOCATION</i>		<i>1-day mm/day</i>	<i>2-day mm/day</i>	<i>3-day mm/day</i>	<i>4-day mm/day</i>	<i>7-day mm/day</i>
Eureka	NOAA	140.21	91.44	68.88	57.30	42.06
	RCP 4.5	172.97	118.04	88.67	75.36	55.58
	RCP 8.5	189.50	140.80	103.22	85.40	61.09
Redding	NOAA	185.32	123.75	95.71	80.47	55.47
	RCP 4.5	198.84	136.41	104.23	90.39	62.60
	RCP 8.5	207.40	141.53	110.81	93.78	71.22
Sacramento	NOAA	121.31	73.76	54.86	44.50	31.09
	RCP 4.5	141.37	95.58	70.00	58.27	39.41
	RCP 8.5	148.79	95.99	74.68	61.00	45.10
San Francisco	NOAA	124.36	74.98	55.47	45.72	32.31
	RCP 4.5	141.70	90.23	68.35	56.21	37.98
	RCP 8.5	147.84	83.90	64.70	54.67	39.35
San Jose	NOAA	89.61	56.69	42.67	34.75	24.38
	RCP 4.5	91.41	59.10	46.52	37.42	28.04
	RCP 8.5	105.26	70.34	53.57	46.85	34.60
Fresno	NOAA	74.98	45.72	32.92	27.43	18.90
	RCP 4.5	81.34	52.31	38.61	31.41	20.94
	RCP 8.5	84.31	56.04	41.80	35.09	25.31
Monterey	NOAA	105.46	67.67	52.43	43.28	29.87
	RCP 4.5	114.63	73.74	56.77	46.95	33.06
	RCP 8.5	119.70	76.76	57.75	48.93	36.83
Santa Barbara	NOAA	176.17	112.78	86.56	71.93	48.77
	RCP 4.5	188.34	125.40	99.82	88.17	60.70
	RCP 8.5	211.95	135.88	110.89	100.93	69.14
Ventura	NOAA	165.20	109.12	84.73	71.32	48.16
	RCP 4.5	169.79	107.70	87.75	76.19	52.34
	RCP 8.5	181.50	120.64	103.41	85.71	64.56
Los Angeles	NOAA	157.89	102.41	80.47	67.06	45.11
	RCP 4.5	169.39	115.15	93.96	81.55	51.64
	RCP 8.5	162.22	114.43	96.06	85.21	64.06
Riverside	NOAA	105.46	68.28	51.21	41.45	27.43
	RCP 4.5	104.61	69.87	52.93	44.35	27.92
	RCP 8.5	107.55	71.51	54.69	44.48	29.79
Palm Springs	NOAA	114.60	70.10	51.21	40.23	25.60
	RCP 4.5	126.22	75.86	56.97	46.38	28.02
	RCP 8.5	132.55	81.91	63.77	51.26	33.82

Irvine	NOAA	120.70	76.81	58.52	48.16	31.70
	RCP 4.5	111.23	74.22	58.01	51.75	32.56
	RCP 8.5	130.08	84.07	67.26	57.25	40.17
Temecula	<i>NOAA</i>	166.42	106.68	79.86	68.28	46.94
	<i>RCP 4.5</i>	187.46	121.21	94.22	80.75	52.06
	<i>RCP 8.5</i>	188.48	128.21	98.03	88.31	63.62
Escondido	<i>NOAA</i>	126.80	81.08	63.40	53.04	35.36
	<i>RCP 4.5</i>	136.92	88.71	67.56	56.05	37.35
	<i>RCP 8.5</i>	139.90	93.05	74.96	62.04	44.88
San Diego	<i>NOAA</i>	90.22	54.86	42.06	34.75	23.77
	<i>RCP 4.5</i>	96.59	65.26	49.95	41.17	26.14
	<i>RCP 8.5</i>	109.12	74.00	54.92	43.63	31.66

Table B-3. 100-yr Return Period Intensity-Duration-Frequency curves based on historical records (NOAA) and future climate (RCP 4.5 and RCP 8.5). The values in the table correspond to the solid lines in Figures 7 and 10. The storm durations indicated are the ones for which NOAA provide the estimates.

<i>100-year Return Period</i>						
<i>LOCATION</i>		<i>1-day mm/day</i>	<i>2-day mm/day</i>	<i>3-day mm/day</i>	<i>4-day mm/day</i>	<i>7-day mm/day</i>
Eureka	NOAA	156.67	101.80	76.81	63.40	46.33
	RCP 4.5	195.87	132.00	98.25	83.83	62.30
	RCP 8.5	217.38	165.12	119.57	98.39	70.06
Redding	NOAA	204.22	135.94	105.46	88.39	61.57
	RCP 4.5	218.00	150.56	115.23	100.52	68.92
	RCP 8.5	228.86	153.77	121.17	101.84	79.06
Sacramento	NOAA	136.55	82.30	60.96	49.38	34.14
	RCP 4.5	161.28	110.22	79.24	66.52	44.64
	RCP 8.5	168.65	106.32	82.85	67.39	49.95
San Francisco	NOAA	142.04	85.34	62.79	51.82	35.97
	RCP 4.5	164.26	104.17	77.84	64.53	42.50
	RCP 8.5	168.08	92.77	71.76	59.88	42.19
San Jose	NOAA	103.63	64.62	48.16	39.62	27.43
	RCP 4.5	104.61	66.00	52.14	42.78	31.96
	RCP 8.5	120.43	79.20	59.61	53.12	38.98
Fresno	NOAA	85.34	51.82	37.80	31.09	21.34
	RCP 4.5	92.87	60.19	44.72	36.07	23.96
	RCP 8.5	96.62	64.03	48.47	39.88	29.20
Monterey	NOAA	121.92	77.42	59.13	49.38	34.14
	RCP 4.5	133.72	85.13	63.90	53.17	38.11
	RCP 8.5	138.92	87.48	64.43	55.24	41.75
Santa Barbara	NOAA	195.68	126.19	97.54	80.47	54.86
	RCP 4.5	210.45	141.20	114.21	101.52	70.38
	RCP 8.5	234.34	149.30	124.80	113.57	76.86
Ventura	NOAA	180.44	120.09	93.88	79.25	53.64
	RCP 4.5	181.77	115.17	95.28	83.15	57.15
	RCP 8.5	193.64	131.89	116.90	95.80	73.26
Los Angeles	NOAA	179.22	116.43	91.44	76.20	51.82
	RCP 4.5	196.07	132.96	109.11	95.11	60.47
	RCP 8.5	177.50	125.57	107.05	96.81	75.81
Riverside	NOAA	120.09	78.03	58.52	47.55	31.70
	RCP 4.5	118.41	78.24	59.46	50.28	31.55
	RCP 8.5	120.00	79.58	60.63	49.37	33.46
Palm Springs	NOAA	134.11	82.30	60.35	47.55	30.48
	RCP 4.5	147.65	88.61	66.96	55.06	33.27
	RCP 8.5	153.82	94.73	75.18	60.17	40.63

Irvine	NOAA	137.16	87.78	67.06	54.86	35.97
	RCP 4.5	124.44	83.58	65.75	58.50	36.42
	RCP 8.5	147.25	96.12	77.55	65.17	45.98
Temecula	<i>NOAA</i>	188.37	123.14	93.27	80.47	55.47
	<i>RCP 4.5</i>	214.92	140.70	110.63	95.45	62.35
	<i>RCP 8.5</i>	211.41	146.70	113.00	103.39	76.40
Escondido	<i>NOAA</i>	143.26	92.66	72.54	60.35	40.84
	<i>RCP 4.5</i>	155.95	101.78	76.82	63.40	43.26
	<i>RCP 8.5</i>	158.02	105.79	85.60	70.38	52.55
San Diego	<i>NOAA</i>	99.97	61.57	46.94	38.40	26.21
	<i>RCP 4.5</i>	108.27	75.48	57.76	46.85	29.08
	<i>RCP 8.5</i>	122.84	86.23	63.41	50.17	36.24